atmosphere

Article

Joint Probability Distribution of Extreme Wind Speed and Air Density Based on the Copula Function to Evaluate Basic Wind Pressure

Lianpeng Zhang [1,†], Zeyu Zhang [1,†], Chunbing Wu [2], Xiaodong Ji [1,*], Xinyue Xue [1], Li Jiang [1] and Shihan Yang [1]

[1] School of Soil and Water Conservation, Beijing Forestry University, Qinghua East Road 35, Beijing 100083, China; zlpneverstops@bjfu.edu.cn (L.Z.); zhangzeyu1997@bjfu.edu.cn (Z.Z.); xuexinyue@bjfu.edu.cn (X.X.); jiangli@bjfu.edu.cn (L.J.); y199992@bjfu.edu.cn (S.Y.)

[2] East China Electric Power Design Institute Co., Ltd. of China Power Engineering Consulting Group, Shanghai 200063, China; wcb19951128@163.com

* Correspondence: jixiaodong@bjfu.edu.cn

† These authors contributed equally to this work.

Abstract: To investigate an appropriate wind load design for buildings considering dynamic air density changes, classical extreme value and copula theories were utilized. Using wind speed, air temperature, and air pressure data from 123 meteorological stations in Shandong Province from 2004 to 2017, a joint probability distribution model was established for extreme wind speed and air density. The basic wind pressure was calculated for various conditional return periods. The results indicated that the Gumbel and Gaussian mixture model distributions performed well in extreme wind speed and air density fitting, respectively. The joint extreme wind speed and air density distribution exhibited a distinct bimodal pattern. The higher the wind speed was, the greater the air density for the same return conditional period. For the 10-year return period, the air density surpassed the standard air density, exceeding 1.30 kg/m^3. The basic wind pressures under the different conditional return periods were more than 10% greater than those calculated from standard codes. Applying the air density based on the conditional return period in engineering design could enhance structural safety regionally.

Keywords: extreme wind speed; air density; copula models; joint probability distribution function; basic wind pressure

Citation: Zhang, L.; Zhang, Z.; Wu, C.; Ji, X.; Xue, X.; Jiang, L.; Yang, S. Joint Probability Distribution of Extreme Wind Speed and Air Density Based on the Copula Function to Evaluate Basic Wind Pressure. *Atmosphere* **2024**, *15*, 1437. https://doi.org/10.3390/atmos15121437

Academic Editor: Stephan Havemann

Received: 23 October 2024
Revised: 22 November 2024
Accepted: 26 November 2024
Published: 29 November 2024

1. Introduction

In recent years, influenced by global warming and climate change, the frequency of natural disasters has increased significantly [1,2]. Among the major natural disasters, wind-related events often result in severe casualties and economic losses [3–5]. For instance, Hurricane Katrina in August 2005 caused 2541 deaths and economic losses reaching USD 110 billion in the USA. Cyclone Sidr in November 2007 resulted in 4234 deaths and economic losses reaching USD 1.7 billion in Bangladesh [6]. In May 2008, Cyclone Nargis devastated Myanmar, causing a staggering 138,366 deaths and economic losses reaching approximately USD 10 billion [7]. More recently, in 2019, Super Typhoon Lekima affected 14.024 million people in China, resulting in direct economic losses of CNY 53.72 billion [8]. In 2022, the 12th typhoon "Meihua" will land northward, bringing rainstorms and floods to the northeast again, disturbing people's lives and even endangering public life and property safety [9]. Ensuring the safety and reliability of infrastructure under the influence of strong winds, or at least minimizing losses, has remained a critical task in wind and civil engineering projects, especially for wind-sensitive structures such as long-span bridges and high-rise buildings [10]. With the increase in high-rise and long-span structures, as well as supertall buildings, determining the basic wind pressure for different return periods is essential for wind-resistant designs, wind load calculation, risk assessment, and disaster mitigation efforts [11].

Wind-related disasters often involve extreme wind speed (v), which serves as a critical parameter for determining the basic wind pressure under various return periods in building design [12]. Typically, two methods are employed to establish wind speed distributions: the time series method and the statistical analysis method [13]. In the statistical analysis method, the utilization of a limited number of parameters provides a more intuitive representation of the distribution of v. Within this context, identifying the most suitable probability density function (PDF) from historical v data is important [14]. In recent years, numerous domestic and foreign scholars have investigated the probability distribution and parameter estimation of v. For instance, Bong-Hee Lee employed Gumbel and Weibull distributions to analyze the daily maximum wind speed and monthly maximum wind speed at 15 wind farms in South Korea from 2005 to 2007. They concluded that the Gumbel distribution consistently outperformed the Weibull distribution [15]. Simiu statistically analyzed v at twenty meteorological stations across the United States. Their findings revealed that 83% of the stations exhibited annual maximum wind speed sequences that followed a Type I extreme value distribution [16]. Escalante-Sandoval Carlos Agustín proposed the use of six mixed probability distribution models, namely, the mixed Gumbel (MG), mixed generalized extreme value (MGEV), and mixed reverse Weibull (MRW) distribution models, to analyze wind speed data spanning 9 to 56 years from multiple meteorological stations in the Netherlands. Parameter estimation was conducted using the maximum likelihood estimation method. The findings revealed that the use of mixed distributions could yield reduced fitting errors. Specifically, 40% of the samples followed the MRW distribution, while another 40% followed the mixed Gumbel-reverse Weibull (G-RW) distribution [17]. Fatih Tosunoğlu utilized six commonly used probability distribution models, namely, the Gamma, Weibull, and generalized extreme value (GEV) models, along with three parameter estimation methods, including moment and maximum likelihood estimation methods, to determine annual maximum wind speed data from Turkey. The fitting performance was assessed through the Akaike information criterion (AIC), Anderson–Darling (AD), Cramer–von Misses (CvM), and Kolmogorov–Smirnov (K-S) test methods. The findings indicated that the data from 40% of the meteorological stations followed the GEV distribution, while the data from 30% of the stations followed the logistic distribution [18]. Notably, employing statistical methods based on probability density distributions to simulate the distribution of v has been widely validated and applied.

In numerous prior investigations concerning the determination of design wind speeds for architectural structures under various return periods, the air density (ρ) has often been treated as a constant, with a value of 1.225 kg/m^3 [19,20] or 1.25 kg/m^3 [21]. However, it is crucial to acknowledge that this standardized ρ value corresponds to specific atmospheric conditions, notably, at sea level, with a temperature of 15 °C and a pressure of 1013 hPa, in which the ρ reaches 1.225 kg/m^3 [22]. Numerous factors influence ρ variations, including the altitude, temperature, pressure, and humidity, leading to spatial and temporal fluctuations. Given the considerable variation in elevation across China, most regions exhibit air densities lower than the standard value [23]. Differences exceeding 10% of the standard ρ have been observed in the northwestern, northern, and southwestern regions, with the maximum deviation surpassing 70% [24]. The complex terrain and notable climatic diversity contribute to spatial and temporal differences in the ρ distribution, challenging the assumption of a uniform ρ in practical applications. Although scholars have begun to acknowledge the role of ρ variation in influencing wind loads on structures [25], systematic investigations into the ρ remain scarce. Furthermore, research suggests that the ρ is subject to a continuous stochastic process [26], highlighting uncertainties regarding the potential correlation between the ρ and wind speed.

The copula function, due to its excellent flexibility and diversity, has been widely applied in various research fields [27,28]. It effectively provides the construction of joint functions for random variables from different marginal distributions, independently considering the correlation between variables [29,30]. The introduction of the copula function has greatly simplified the extension of joint distribution functions from two to three dimensions and beyond. Currently, scholars both domestically and internationally have constructed joint distribution models of v with various random variables, such as the wind direction, rain intensity, and rainfall, based on copula theory, achieving notable results. With the use of wind and wave observation data from the Shidao Station from 2011 to 2019, statistical analyses were conducted with both mixed and single copula models to evaluate the return period and conditional probability of wind and wave events. The findings indicated that mixed copula models more accurately capture the complex dependency structures between ocean parameters than single copula models can. Additionally, the joint return periods and conditional probabilities obtained using mixed copula models demonstrated greater reliability [31]. Within the context of the occurrence of v and extreme temperatures, Wang established an Archimedean copula joint distribution model using 30 years of v and extreme temperature data and calculated the combined values under joint return periods of these two variables [32].

The above indicates that research on v is relatively advanced, with many methods and models available, providing reliable guidance for calculating the basic wind pressure for various return periods. However, in recent architectural designs, the ρ is typically assumed as exhibiting a fixed value of 1.25 kg/m^3, with little consideration given to the impact of the statistical characteristics of the ρ in the field of structural engineering. Therefore, the main questions considered in this study are as follows: How can the v and ρ be linked? How does the ρ under the joint distribution and conditional probability influence the basic wind pressure? To address these questions, we selected Shandong Province, China, as the study area, utilizing data from 123 long-term meteorological observation stations. The optimal marginal distributions for the v and concurrent ρ were identified. Based on copula theory, a joint probability distribution model for the v and concurrent ρ was constructed. Then, conditional return periods were derived from this model. This study aimed to elucidate the differences between basic wind pressure values considering the ρ under various conditional return periods and those calculated according to standard codes. This study provides both data and theoretical support for wind load design in architecture.

2. Data and Methods

2.1. Study Area

Shandong Province is an eastern coastal province of China located between 114°21′ and 122°43′ E longitude and 34°22′ and 38°24′ N latitude (Figure 1) [33]. The province encompasses 17 cities, covering a total area of over 151,100 square kilometres. Plains account for 55% of the total area, with mountains and hills accounting for 15.5% and 13.2%, respectively, of the total area. The climate can be classified as a warm temperate with semihumid monsoon climate influenced by both continental and maritime monsoons. Winters are cold and dry, while summers are hot and humid, with significant seasonal variations and regional differences. The annual average temperature ranges from 11 °C to 14 °C, and the annual precipitation ranges from 550 to 950 mm [34]. Shandong is prone to various natural disasters, rendering it one of the most affected regions in China. It frequently exhibits droughts, seasonal heavy rains, floods, hailstorms, thunderstorms, typhoons, and geological disasters such as earthquakes and mudslides [35].

2.2. Data

The data utilized in this study were obtained from surface meteorological observation stations managed by the China Meteorological Administration [36]. The locations and elevations of 123 meteorological observation stations in Shandong Province, China, are shown in Figure 1. The observation data comprised air pressure (P) and air temperature (T_a) recorded hourly at a height of 2 m, along with the maximum 10 min average wind speed (v) recorded hourly at a height of 10 m from 2004 to 2017. Data gaps and evident outliers, such as values of 999,999, were excluded. Four typical sites within the research area were chosen for comparison based on their diverse geographic locations and elevations, as shown in Figure 1. Detailed information on these typical sites is provided in Table 1. In conducting wind load calculations, the selection of Anqiu, Qingdao, Tancheng, and Rizhao from the 123 meteorological stations in Shandong Province is justified by the distinct climatic conditions and geographical features represented by these 4 regions. Qingdao, as a coastal city, is subject to significant marine winds, providing critical data on coastal wind patterns. In contrast, Anqiu and Tancheng are situated inland, making them suitable for studying the influences of continental climate. Rizhao, with its unique combination of coastal and inland characteristics, further enhances the understanding of wind load variations across different environments. This strategic selection allows for a more comprehensive and representative assessment of wind load characteristics in diverse regional contexts.

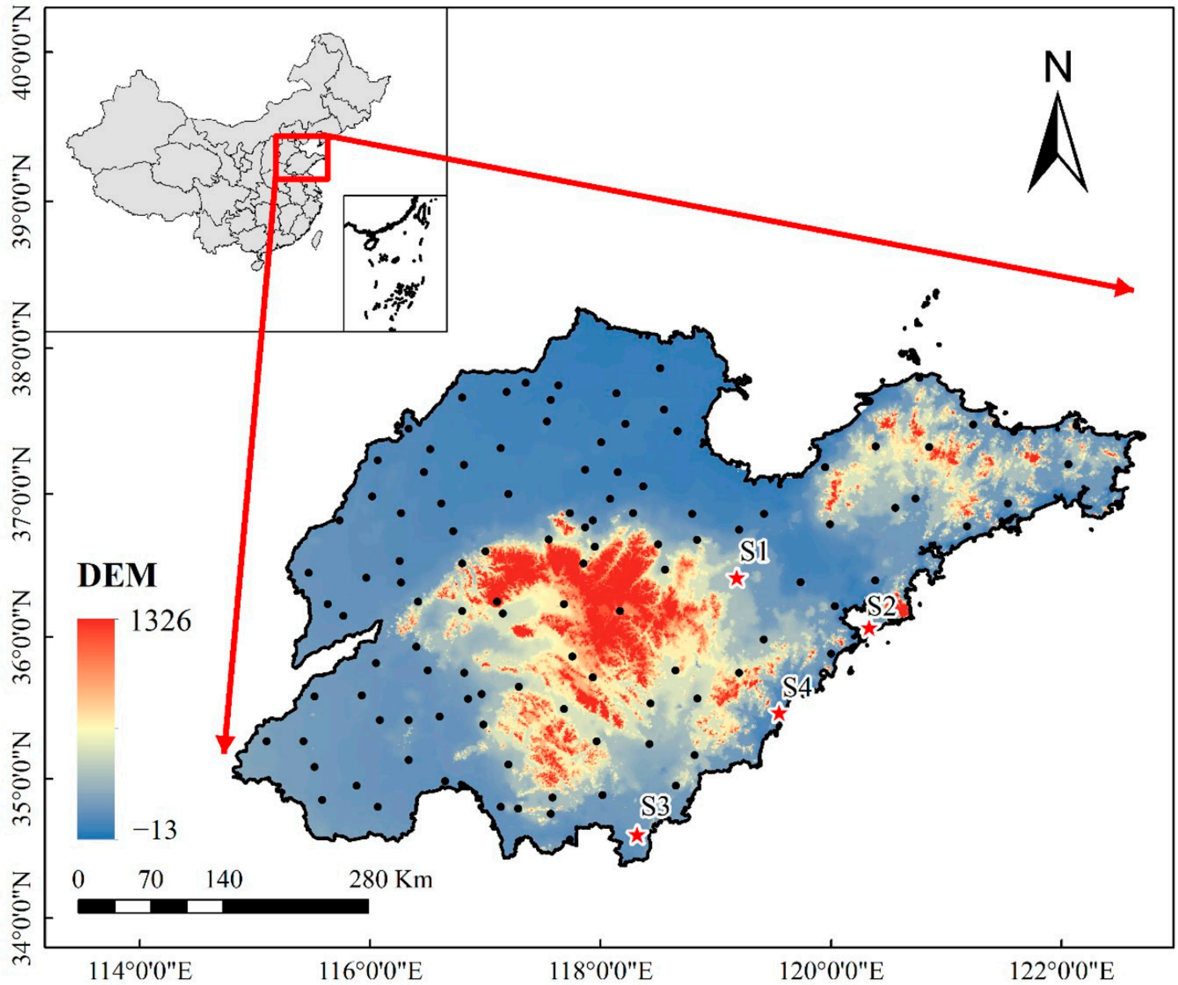

Figure 1. Distribution of the 123 meteorological stations (black dots), 4 typical sites (red stars), and the study area with elevation (*el*).

Table 1. Geographical location and elevations of the six typical sites.

Typical Site	Site Name	Lat. (°)	Lon. (°)	*el* (m)
S1	Anqiu	36.4167	119.1833	62.7
S2	Qingdao	36.0667	120.3333	76.0
S3	Tancheng	34.6	118.3167	37.2
S4	Rizhao	35.4667	119.55	16.1

2.3. Calculation of the Air Density

According to China's "Load Code for the Design of Building Structures." [37,38], the measurement height for the basic wind pressure is standardized at 10 m. Based on the barometric pressure, Equations (1) and (2) [24] can be used to convert the air pressure and temperature, respectively, recorded at a height of 2 m into values at the standard height of 10 m by using Equations (1) and (2), respectively.

$$P(h_g) = P(h_0)(1 - \frac{0.0065 \cdot \Delta h}{T_a(h_0)})^{5.255877} \quad (1)$$

$$T_a(h_g) = T_a(h_0) - 0.0065 \cdot \Delta h \quad (2)$$

where h_0 denotes the original elevation of the meteorological data, h_g is the target height after interpolation, and Δh denotes the difference in elevation (m).

With the use of the extrapolated temperature and pressure at the hub height, the ideal gas law (3) can be applied to compute the ρ values [39,40] as follows:

$$\rho = \frac{P}{G \cdot T_a} \quad (3)$$

where ρ is the air density, P is the air pressure, T_a is the air temperature, and G is the gas constant for dry air, with a value of 287.058 J·(kg K)$^{-1}$.

2.4. Probability Density Function of Air Density and Extreme Wind Speed

Theoretical distributions were employed to derive continuous distributions for the modelled ρ and v. The considered PDFs for the ρ included the two-parameter Weibull distribution, two-parameter Gamma distribution, three-parameter Burr distribution, three-parameter GEV distribution [36], and two-dimensional Gaussian mixture model (GMM) [41]. We selected the monthly maximum wind speed as a measure of the v. The corresponding PDFs included the two-parameter Gumbel, two-parameter Gamma, three-parameter Burr, and two-parameter Weibull distributions [42–44]. The parameters for each theoretical distribution were estimated using the maximum likelihood estimation method. Tables 2 and 3 provide the number of parameters and equations for the four theoretical distributions for the ρ and v, respectively.

Table 2. Number of parameters and equations for the four one-component probability density functions for the air density.

Pdf	Parameter	Probability Density Function Equation
GEV	$\sigma; \gamma; \lambda$	$F_{GEV}(x) = \begin{cases} \exp\left[-(1+\gamma z)^{-\frac{1}{\gamma}}\right] & \gamma \neq 0 \\ \exp(-\exp(-z)) & \gamma = 0 \end{cases}$ $z = \frac{x-\lambda}{\sigma}$
Gamma	$\sigma; \gamma$	$F_G(x) = \frac{\Gamma_{v/\gamma}(\sigma)}{\Gamma(\sigma)}$
Burr	$\sigma; \gamma; h$	$F_B(x) = 1 - \left[1 + \left(\frac{x}{\gamma}\right)^h\right]^{-\sigma}$
Weibull	$\sigma; \gamma$	$F_W(x) = 1 - \exp\left[-\left(\frac{x}{\sigma}\right)^\gamma\right]$
GMM	$\theta; \sigma_1; \sigma_2; \lambda_1; \lambda_2$	$f_{GMM}(x) = \theta \frac{1}{\sqrt{2\pi}\sigma_1} \exp\left(-\frac{(x-\lambda_1)^2}{2\sigma_1^2}\right) + (1-\theta)\frac{1}{\sqrt{2\pi}\sigma_2} \exp\left(-\frac{(x-\lambda_2)^2}{2\sigma_2^2}\right) \quad \theta \in [0,1]$

where σ is the scale parameter, λ is the position parameter, γ is the shape parameter, h is the second shape parameter, $\Gamma(\,)$ is the Gamma function, θ denotes the prior probability of the second normal distribution, σ_1 is the scale parameter, σ_2 is the scale parameter of the second normal distribution, λ_1 is the position parameter, and λ_2 is the scale parameter of the second normal distribution.

Table 3. Number of parameters and equations for the four one-component probability density functions for the extreme wind speed.

Pdf	Parameter	Cumulative Probability Function	Probability Density Function Equation
Gumbel	$\sigma; \lambda$	$F_{Gu}(v)= \exp\left\{-\exp\left[-\frac{(v-\lambda)}{\sigma}\right]\right\}$	$f_{Gu}(v_m) = \frac{\exp\left\{-\exp\left[-\frac{(v-\lambda)}{\sigma}\right]-\frac{(v-\lambda)}{\sigma}\right\}}{\sigma}$
Gamma	$\sigma; \gamma$	$F_G(v) = \frac{\Gamma_{v/\gamma}(\sigma)}{\Gamma(\sigma)}$	$f_G(v) = \frac{x^{\gamma-1}}{\sigma^\gamma\Gamma(\sigma)}\exp\left(-\frac{v}{\gamma}\right)$
Burr	$\sigma; \gamma; h$	$F_B(v)= 1-\left[1+\left(\frac{v}{\gamma}\right)^h\right]^{-\sigma}$	$f_B(v) = \frac{h\sigma\left(\frac{v}{\gamma}\right)^{h-1}}{\gamma\left[1+\left(\frac{v}{\gamma}\right)^h\right]^{\sigma+1}}$
Weibull	$\sigma; \gamma$	$F_W(v)= 1-\exp\left[-\left(\frac{v}{\sigma}\right)^\gamma\right]$	$f_W(v) = \frac{\gamma}{\sigma}\left(\frac{v}{\sigma}\right)^{\gamma-1}\exp\left[-\left(\frac{v}{\sigma}\right)^\gamma\right]$

where σ is the scale parameter, λ is the position parameter, γ is the shape parameter, h is the second shape parameter, $\Gamma(\,)$ is the Gamma function, and $\Gamma_z(\,)$ is the incomplete Gamma function.

Since different goodness-of-fit (GoF) metrics can yield varied fitting evaluation results, four distinct metrics were employed to assess the accuracy of the PDFs fitted to empirical probability density functions (EPDFs). The utilized metrics are the coefficient of determination (R^2) [45], K-S statistic [46], AD test statistic [47], and chi-square test statistic [48], as expressed in Equations (4)–(7), respectively.

$$R^2 = 1 - \frac{\sum_{i=1}^{n}\left(F_i-\hat{F}_i\right)^2}{\sum_{i=1}^{n}\left(F_i-\overline{F}\right)^2} \tag{4}$$

where F_i is the value of the ith empirical cumulative distribution function (ECDF), $\hat{F}_i$ is the estimated cumulative distribution function (CDF) of the values of the ith ECDF, and $\overline{F_i}$ denotes the mean value of F_i.

$$D = \underset{-\infty<v<+\infty}{Sup}\left|F_n^*(v)-F_n(v)\right| \tag{5}$$

where $Fn(v)$ denotes the empirical distribution function values, $Fn^*(v)$ denotes the theoretical distribution function values, and n denotes the sample size.

$$A_n^2 = \frac{1}{n}\left[\sum_i^n(1-2i)\log z_i - (2i-1-2n)\log(1-z_i)\right] - n \tag{6}$$

where z_i is the distribution function value $F(v_i)$ corresponding to v_i.

$$\chi^2 = \frac{\sum_{i=1}^{n}\sum_{j=1}^{m}\left(K_{ij}-L_{ij}\right)}{L_{ij}} \tag{7}$$

where n denotes the number of sample points, m denotes the number of different attributes, K_{ij} denotes the empirical frequency values, and L_{ij} denotes the theoretical frequency values.

2.5. Joint Probability Density Function of Extreme Wind Speed and Air Density

The joint probability density function (JPDF) of the ρ and v can be characterized by a copula function. The copula function is essentially a connection function that aims to link the distribution functions of multivariate random variables [49]. The chosen copula function model is the Clayton copula joint distribution model, which is characterized by a notable lower tail dependence and no upper tail dependence [32,50]. The distribution function of the bivariate Clayton copula can be expressed as follows (Equation (8)):

$$C[U_{u_1}(u_1), U_{u_2}(u_2)] = \left\{[U_{u_1}(u_1)]^{-\varphi} + [U_{u_2}(u_2)]^{-\varphi} - 1\right\}^{-\frac{1}{\varphi}} \tag{8}$$

where $Uu_1(u_1)$ is the marginal distribution of the first variable, specifically the marginal distribution of the extreme wind speed; $Uu_2(u_2)$ denotes the marginal distribution of the second variable, specifically the marginal distribution of ρ; and φ is the parameter of the Clayton copula.

The corresponding PDF can be expressed as Equation (9).

$$c[U_{u_1}(u_1), U_{u_2}(u_2)] = (1+\varphi)\left\{[U_{u_1}(u_1)]^{-\varphi} + [U_{u_2}(u_2)]^{-\varphi} - 1\right\}^{-\frac{1}{\varphi}-2}[U_{u_1}(u_1)U_{u_2}(u_2)]^{-\varphi-1} \tag{9}$$

2.6. Return Period and Basic Wind Pressure Calculation Model

Under the premise of two variables, the conditional probability distribution refers to the probability distribution of one variable given a specific condition of the other variable. When the v exceeds a specific value v^*, the conditional probability of the ρ can be expressed as Equation (10).

$$P(U_2 \le u_2 | U_1 > u_1^*) = \frac{P(U_2 \le u_2 \cap U_1 > u_1^*)}{P(U_1 > u_1^*)} = \frac{U_2(u_2) - C[U_{u_1}(u_1^*), U_{u_2}(u_2)]}{1 - U_1(u_1^*)} \tag{10}$$

where $Uu_1(u_1)$ denotes the marginal distribution of the first variable, specifically the marginal distribution of the extreme wind speed, and $Uu_2(u_2)$ denotes the marginal distribution of the second variable, specifically the marginal distribution of ρ. Moreover, $C[]$ is the copula function, specifically the Clayton copula.

The corresponding conditional return period can be expressed as follows (Equation (11)):

$$T^* = \frac{1}{1 - P(U_2 \le u_2 | U_1 > u_1^*)} \tag{11}$$

where T^* is the conditional return period.

Basic wind pressure is one of the fundamental parameters for calculating wind loads on primary or enclosure structures. The determination of the basic wind pressure is crucial for assessing the wind loads acting on a given structure. According to Chinese load code GB50009-2012 [51], once the basic wind speed for different return periods is obtained, the wind load can be calculated, as expressed in Equation (12).

$$w_0 = \frac{1}{2}\rho v_0^2 \tag{12}$$

where w_0 is the basic wind pressure, ρ is the air density, and v_0 is the design wind speed.

3. Results

3.1. Marginal Distribution of Extreme Wind Speed and Air Density

Notably, the GoF values between the theoretical and empirical distributions of the v were obtained and evaluated, and the results are shown in Figure 2. Among the four evaluated PDFs, except for the Weibull distribution, the median R^2 values of all the other PDFs indicated high precision, i.e., the values are greater than 0.90 (Figure 2a), with the gamma distribution performing the best, with a value of 0.95. Regarding the K-S, AD, and chi-square test statistics, a smaller value indicates a better fit. When comparing the median D values, all four PDFs exhibited values less than 0.20, with the Gumbel distribution performing the best, with a value of 0.05. In terms of the AD test statistic, except for the Weibull distribution, the remaining three PDFs exhibited values below 0.60, with the Gumbel distribution again performing the best, yielding a value of 0.32. In regard to the chi-square test statistic, except for the Weibull distribution, which exhibited a value as high as 18.03, the other PDFs demonstrated values below 6.00, with the Gumbel distribution performing the best, yielding a value of 4.54. Therefore, it could be concluded that the Gumbel distribution could best reproduce the v in the study area. We calculated the relevant parameters for fitting the marginal distribution of wind speed at four stations (Table 4).

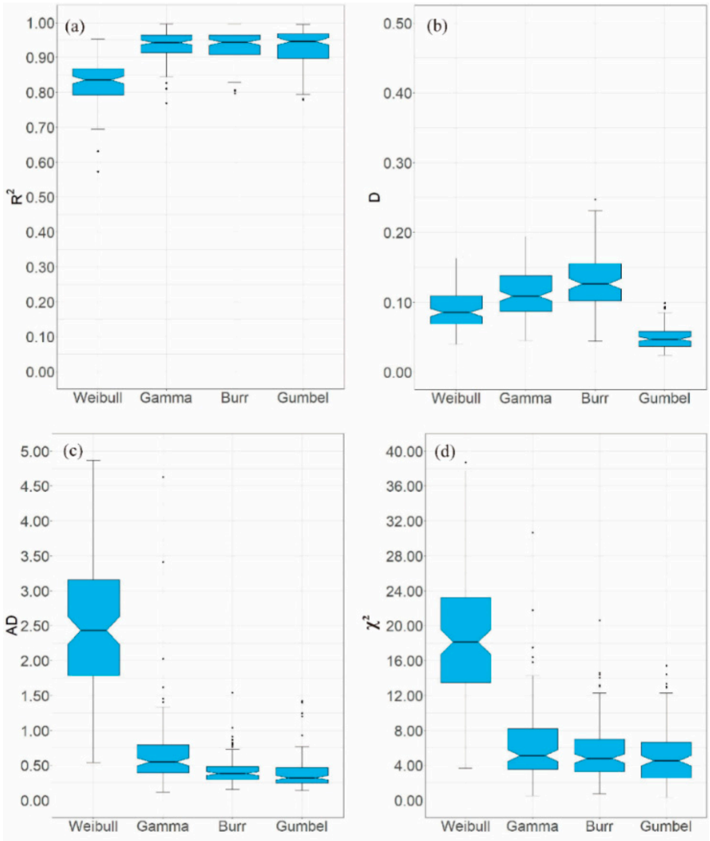

Figure 2. GoF analysis of the match of the four PDFs to the empirical distributions of extreme wind speed with respect to various assessment metrics, including (**a**) R^2, (**b**) D, (**c**) AD, and (**d**) χ^2.

Table 4. Parameter estimates of four probability distributions of the four typical sites based on the monthly maximum wind speed series.

Site	Weibull		Gamma		Burr			Gumbel	
	σ	γ	σ	γ	σ	γ	h	σ	λ
S1	11.926	4.996	0.430	25.592	0.881	10.525	9.259	1.846	9.965
S2	15.738	5.415	0.553	26.327	1.549	15.519	7.822	2.578	13.190
S3	11.537	4.730	0.487	21.766	0.999	10.325	7.991	1.919	9.508
S4	11.487	4.175	0.682	15.340	1.926	11.952	5.646	2.345	9.177

.

Figure 3 shows the empirical distributions of the maximum wind speed and the corresponding four optimal fitted theoretical distributions at the four typical locations. The distributions at the four locations exhibited a distinct unimodal pattern. Sites S1, S3, and S4, located in inland areas, demonstrated peak values concentrated at approximately 10.00 m/s. In contrast, Site S2, situated at the edge of the coast, exhibited higher v due to the influence of sea breezes, resulting in a less concentrated peak shape, with peak values primarily varying between 14.00 and 16.00 m/s. Notably, the Gumbel distribution provided a satisfactory fit for the observed v.

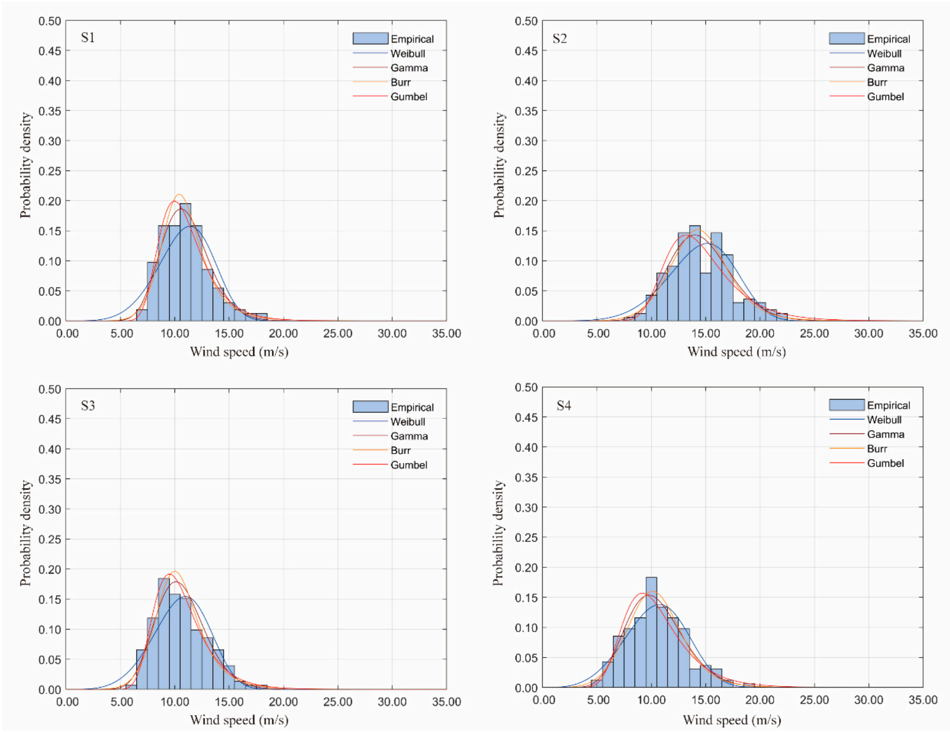

Figure 3. Empirical probability density functions of the extreme wind speed and the four fitted theoretical distributions at the four typical sites at S1, S2, S3, and S4.

To assess the obtained fit of each theoretical distribution to the empirical distribution of the ρ, we selected the coefficient of determination (R^2) (Table 5). The closer the R^2 value is to 1, the better the fit. Compared to the fitting performance for the wind speed, the fitting performance for the ρ was lower. The median R^2 value of the Weibull distribution was less than 0.28, while the GMM distribution attained the highest median R^2 value of 0.70. This is primarily due to the distinct cold and warm seasons in the study area, resulting in a bimodal empirical distribution of the ρ (Figure 4), whereas single-component probability density curves can fit unimodal distributions better. In this study, the gamma distribution demonstrated the best ability to reproduce the ρ in the study area.

Table 5. R^2 values for the fitting accuracy between the empirical distributions and five theoretical distributions of air density under extreme wind speeds.

PDF	R^2			
	25%	50%	75%	Average
Weibull	0.113	0.280	0.376	0.262
Gamma	0.246	0.389	0.447	0.355
Burr	0.267	0.373	0.409	0.347
GEV	0.310	0.427	0.480	0.402
GMM	0.668	0.701	0.776	0.704

The theoretical probability distributions of the ρ were fitted to the empirical distributions at four locations, as shown in Figure 4. The ρ at all four locations primarily varied between 1.10 and 1.40 kg/m^3, exhibiting a bimodal distribution with indistinct peaks. The primary peak reached approximately 1.15 kg/m^3, while the secondary peak reached approximately 1.30 kg/m^3. Additionally, it is clear that the GMM distribution provided a suitable fit for the v. We calculated the relevant parameters for fitting the marginal distribution of air density at the four stations (Table 6).

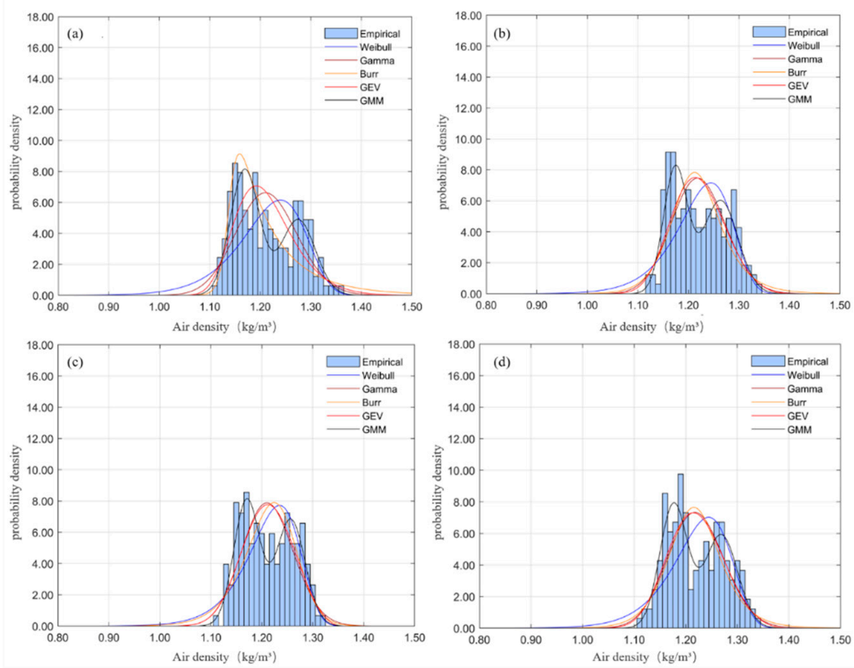

Figure 4. Empirical probability density functions of air density and the fitted four theoretical distributions at the four typical sites at S1 (**a**), S2 (**b**), S3 (**c**), and S4 (**d**).

Table 6. Parameter estimates of four probability distributions of the four typical sites based on the air density series.

Site	Weibull		Gamma		Burr			GEV			GMM				
	σ	γ	σ	γ	σ	γ	h	σ	γ	λ	θ	σ_1	σ_2	λ_1	λ_2
S1	1.249	22.046	0.003	453.342	0.260	1.163	73.817	0.052	−0.158	1.197	0.583	0.029	0.034	1.169	1.275
S2	1.243	25.364	0.002	604.816	0.182	1.161	111.265	0.045	−0.152	1.198	0.480	0.024	0.034	1.174	1.263
S3	1.246	23.394	0.002	510.207	0.321	1.170	67.276	0.049	−0.169	1.197	0.517	0.026	0.028	1.710	1.257
S4	1.247	24.656	0.002	569.557	0.229	1.167	90.568	0.046	−0.161	1.200	0.526	0.027	0.032	1.177	1.269

3.2. Joint Probability Density Distribution of Air Density and Extreme Wind Speed

Based on the optimal marginal distributions of the v and ρ, specifically the Gumbel and GMM distributions, respectively, we selected the Clayton copula joint distribution for the simulation. As shown in Figure 5, the joint distribution exhibited a distinct bimodal pattern. The ρ at the four typical locations ranged from 1.00 to 1.40 kg/m^3. At S1, S3, and S4, the peaks primarily occurred at an ρ of approximately 1.10 kg/m^3 and a wind speed of approximately 10 m/s. However, the peak shapes at S1 and S4 were more concentrated, with S1 indicating a higher primary peak (Figure 5a) and S4 indicating a higher secondary peak, nearly matching the primary peak (Figure 5d). The distance between the primary and secondary peaks at S3 exceeded that at S4 (Figure 5c). Due to its coastal location, S2 exhibited a peak ρ of approximately 1.10 kg/m^3, but the wind speed was approximately 15 m/s (Figure 5b).

As shown, Figure 6 primarily focuses on the CDF, which differs from the PDF. The CDF more intuitively illustrates the joint probability of ρ and v occurring simultaneously. Taking the four sites as examples, for S1 and S4, the probability of ρ exceeding the standard value of 1.25 kg/m^3 is greater than 30.00%, while the probability of v exceeding 10 m/s when ρ is above the standard value is less than 15.00%. For S2, the probability of ρ exceeding the standard value is 34.15%, and the probability of v exceeding 10 m/s under these conditions is 28.66%. For S3, the probability of ρ exceeding the standard value is less than 30.00%, and the probability of v exceeding 10 m/s is less than 5%.

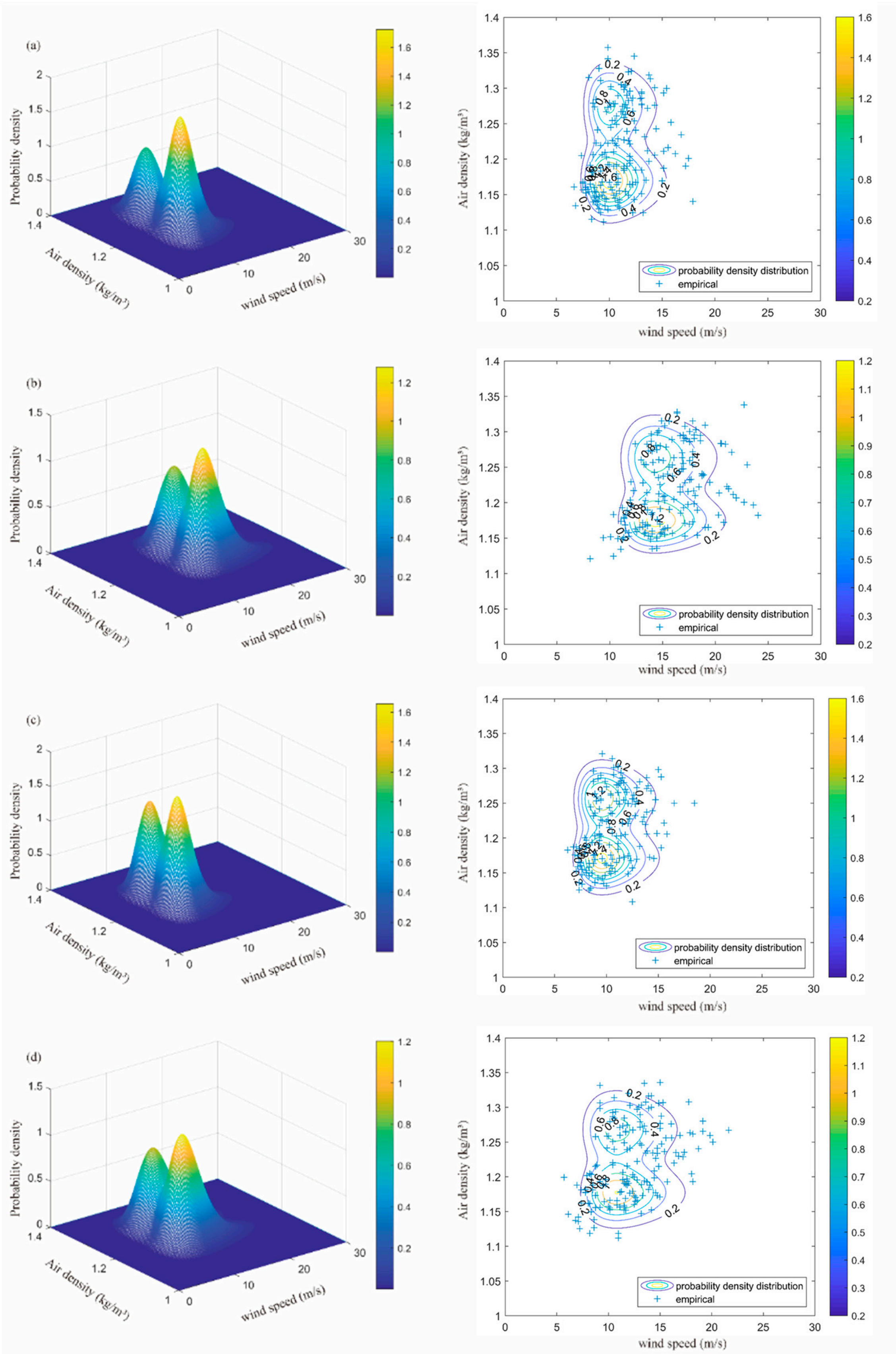

Figure 5. Joint probability density contours and empirical distribution scatter plots for the independent extreme wind speed and air density at S1 (**a**), S2 (**b**), S3 (**c**), and S4 (**d**).

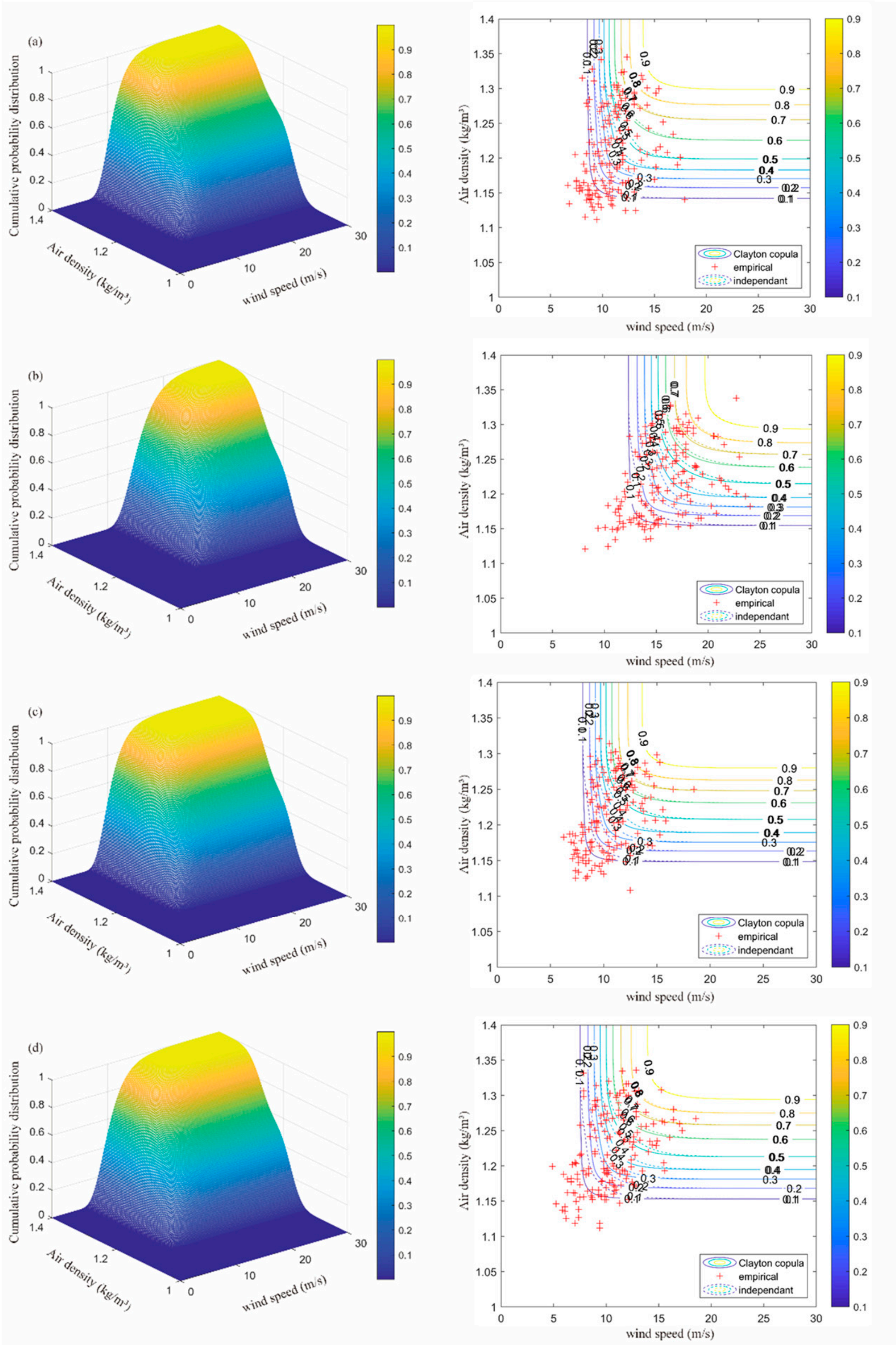

Figure 6. Cumulative probability distribution of the Clayton copula combined with the extreme wind speed and air density at S1 (**a**), S2 (**b**), S3 (**c**), and S4 (**d**).

3.3. Conditional Return Period and Basic Wind Pressure

Adopting S1 as an example, the conditional probability distribution of the ρ at different wind speeds (Figure 7 andFigure 8) and conditional return periods were simulated. The conditional probability of the ρ decreased with increasing wind speed. Additionally, with increasing wind speed, the ρ increased for the same return period. Conversely, at higher wind speeds, the conditional return period decreased for the same ρ.

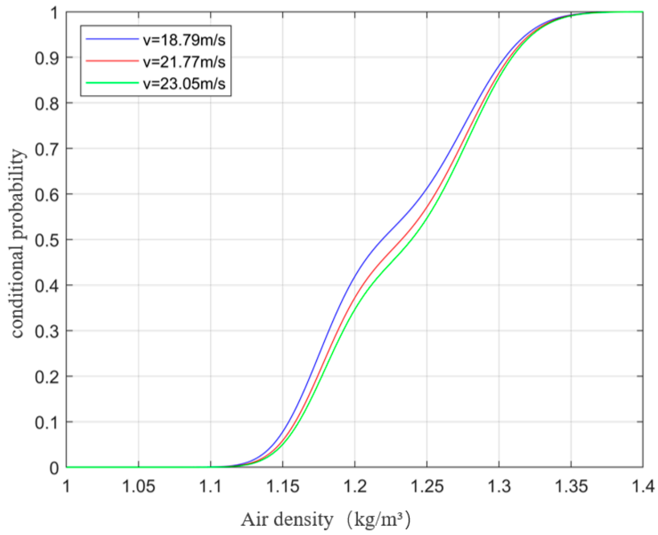

Figure 7. Conditional probability distribution of the air density at the S1 meteorological station under different wind speeds.

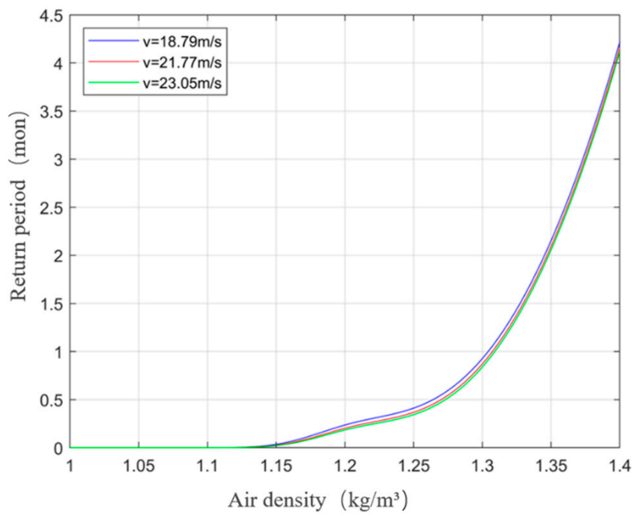

Figure 8. Conditional return period of the air density at the S1 meteorological station under different wind speeds.

By comparing the v and ρ at the four locations under the different return periods (Table 7), it could be observed that for the 10-year return period, the v at both S2 and S4 exceeded 20 m/s. For the 50-year return period, the values at all four typical locations exceeded 20 m/s, and for the 100-year return period, the value at S2 exceeded 30 m/s. Additionally, based on the joint probability density distribution, the ρ exceeded 1.30 kg/m^3 for the 10-year return period, surpassing the standard ρ of 1.25 kg/m^3.

Table 7. Design value of the return period of the air density under extreme wind speed conditions for return periods of 10, 50, and 100 years at the four meteorological stations.

Typical Site	Return Period Wind Speed (m/s)			Return Period Air Density Under Conditional Probability (kg/m^3)		
	10-Year	50-Year	100-Year	10-Year	50-Year	100-Year
S1	18.79	21.77	23.05	1.3628	1.3776	1.3837
S2	25.52	29.68	31.47	1.3386	1.3623	1.3690
S3	18.69	21.78	23.11	1.3314	1.3435	1.3486
S4	20.39	24.18	25.8	1.3462	1.3612	1.3673

Based on the design values under various conditional return periods, which are calculated values from the code based on the altitude considering a fixed ρ value (1.25 kg/m^3), the basic wind pressure values at the four typical locations were calculated (Figure 9). The design values under the various conditional return periods were greater than those specified by the code using a fixed ρ. For the 100-year conditional return period, the wind pressure at S2 exceeded 0.40 kN/m^2, while the basic wind pressure exceeded 0.60 kN/m^2. At the other three locations, the basic wind pressure was less than 0.30 kN/m^2 for the 10-year conditional return period, exceeded 0.30 kN/m^2 for the 50-year conditional return period, and was greater than 0.30 kN/m^2 for the 100-year return period, with that at S4 reaching as high as 0.45 kN/m^2. Although the basic wind pressure at S1 was not the highest, the basic wind pressure under the various conditional return periods was more than 10% higher than the altitude-based calculated value from the code. Similarly, the difference at S2 exceeded 10% for the 100-year return period.

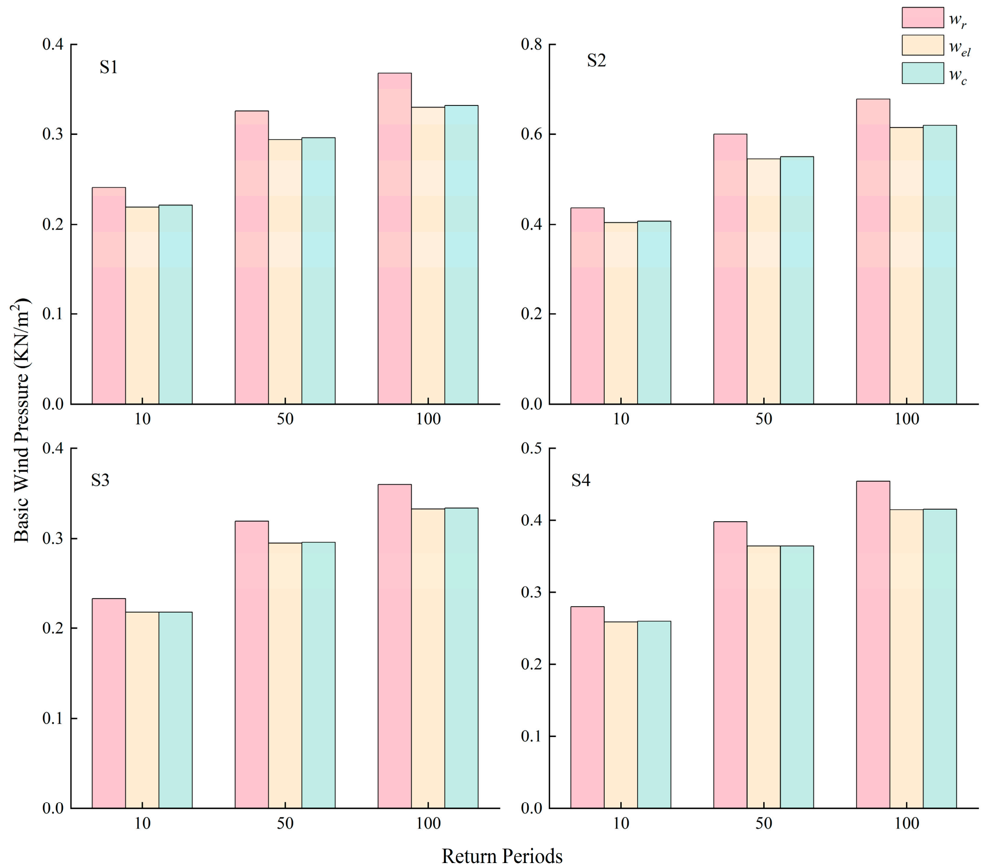

Figure 9. Comparison of the basic wind pressures for the 10-, 50-, and 100-year return periods under the different air densities.

4. Conclusions

Based on wind speed, air temperature, and air pressure data from 123 meteorological stations in Shandong Province from 2004 to 2017, the joint distribution of the extreme wind speed and air density was established using the copula function. This allowed for the assessment of the basic wind pressure under different return periods. The main conclusions of this study are as follows:

- Among the different PDFs used to fit the empirical distributions of the long-term series of the extreme wind speed and air density, the Gumbel distribution demonstrated a superior ability in fitting the extreme wind speed, while the GMM distribution performed well in fitting the air density.

- The joint distribution of the extreme wind speed and air density, which was established using the Clayton copula function, exhibited a typical bimodal pattern. Due to differences in the altitude and geographical location, the four typical sites demonstrated distinct bimodal distributions.
- The conditional return period calculated based on the joint distribution revealed that with increasing wind speed, the conditional probability of the air density decreased, resulting in a higher air density for the same return period. For the 10-year return period, the air density exceeded the standard air density, reaching above 1.30 kg/m^3.
- The basic wind pressures under the different conditional return periods were all greater than those calculated from standard codes, with the maximum at the four typical sites exceeding the standard wind pressure by more than 10%.

The design wind speed and air density are crucial parameters for calculating wind loads on building structures. In this study, more accurate basic wind pressure calculations were achieved based on the joint distribution, providing supporting data and a theoretical basis for the improvement in future wind load standards.

Author Contributions: L.Z.: Conceptualization, Methodology, Software, Investigation, Writing—Original Draft; Z.Z.: Conceptualization, Methodology, Software, Formal Analysis, Writing—Review and Editing; C.W.: Conceptualization, Methodology, Software, Formal Analysis, Visualization; X.J.: Conceptualization, Writing—Review and Editing, Supervision, Project Administration, Funding Acquisition, Data Curation; X.X.: Methodology, Software, Formal Analysis, Visualization; L.J.: Methodology, Software, Visualization; S.Y.: Methodology, Software, Visualization. All authors have read and agreed to the published version of the manuscript.

Funding: The work was supported by the National Natural Science Foundation of China (31570708), the Major Science and Technology Program for Water Pollution Control and Treatment of China (2017ZX07101002-002), and the National Key Scientific and Technological Infrastructure project "Earth System Science Numerical Simulator Facility" (EarthLab).

Institutional Review Board Statement: Not applicable.

Informed Consent Statement: Not applicable.

Data Availability Statement: The data presented in this study are available on request from the corresponding author. The data are not publicly available due to privacy.

Conflicts of Interest: The manuscript was approved by all authors for publication, and they declare that they have no conflicts of interest.

Declaration of Generative AI and AI-Assisted Technologies in the Writing Process: During the preparation of this work, the author(s) used ChatGPT 4.0 in order to improve readability and language. After using this tool/service, the author(s) reviewed and edited the content as needed and take(s) full responsibility for the content of the publication.

References

1. Cappelli, F.; Costantini, V.; Consoli, D. The trap of climate change-induced "natural" disasters and inequality. *Glob. Environ. Change* **2021**, *70*, 102329. [CrossRef]
2. Sloggy, M.R.; Suter, J.F.; Rad, M.R.; Manning, D.T.; Goemans, C. Changing opinions on a changing climate: The effects of natural disasters on public perceptions of climate change. *Clim. Change* **2021**, *168*, 1–26. [CrossRef] [PubMed]
3. Eslamian, S.; Eslamian, F. Types, Definition and Classification of Natural Disasters and Threat Level. In *Handbook of Disaster Risk Reduction for Resilience: New Frameworks for Building Resilience to Disasters*; Springer International Publishing AG: Cham, Switzerland, 2021.
4. Little, A.S.; Priestley, M.; Catto, J.L. Future increased risk from extratropical windstorms in northern Europe. *Nat. Commun.* **2023**, *14*, 4434. [CrossRef] [PubMed]
5. Shen, G.; Zhou, L.; Xue, X.; Zhou, Y. The risk impacts of global natural and technological disasters. *Socio-Econ. Plan Sci.* **2023**, *88*, 101653. [CrossRef]
6. Yang, Q.; Gao, R.; Bai, F.; Li, T.; Tamura, Y. Damage to buildings and structures due to recent devastating wind hazards in East Asia. *Nat. Hazards* **2018**, *92*, 1321–1353. [CrossRef]
7. Tamura, Y.; Cao, S. International Group for Wind-Related Disaster Risk Reduction (IG-WRDRR). *J. Wind Eng. Ind. Aerodyn.* **2012**, *104–106*, 3–11. [CrossRef]

8. Gao, Y.; Zhang, Y.; Lei, L.; Tang, J. Multi-scale characteristics of an extreme rain event in Shandong Province, produced by Typhoon Lekima (2019). *Front. Earth Sci.* **2023**, *10*, 1093545. [CrossRef]
9. Li, Z.; Wang, J.; Wei, C.; Yu, J. Analysis of the Temporal and Spatial Characteristics of PWV and Rainfall with the Typhoon Movement: A Case Study of 'Meihua' in 2022. *Atmosphere* **2023**, *14*, 1313. [CrossRef]
10. Wei, M.; Fang, G.; Zhao, L.; Wang, Z.; Wang, J.; Cao, S.; Ge, Y. Comparative study of typhoon wind hazard estimation in coastal region of China using different wind field parameter models. *J. Wind Eng. Ind. Aerodyn.* **2023**, *236*, 105398. [CrossRef]
11. Du, K.; Chen, B. A hybrid semi-supervised regression based machine learning method for predicting peak wind loads on a group of buildings. *Eng. Struct.* **2023**, *275*, 115245. [CrossRef]
12. Wu, F.; Gong, J.; Yu, H. Comparative study on the performances of moment-based models with almost no monotonic limit in the non-Gaussian wind pressure extreme value estimation. *Structures* **2024**, *64*, 106635. [CrossRef]
13. Shi, H.; Dong, Z.; Xiao, N.; Huang, Q. Wind Speed Distributions Used in Wind Energy Assessment: A Review. *Front. Energy Res.* **2021**, *9*, 769920. [CrossRef]
14. Aljeddani, S.M.; Mohammed, M.A. An extensive mathematical approach for wind speed evaluation using inverse Weibull distribution. *Alex. Eng. J.* **2023**, *76*, 775–786. [CrossRef]
15. Lee, B.; Ahn, D.; Kim, H.; Ha, Y. An estimation of the extreme wind speed using the Korea wind map. *Renew. Energy* **2012**, *42*, 4–10. [CrossRef]
16. Simiu, E.; Filliben, J.J. Probability distributions of extreme wind speeds. *J. Struct. Div.* **1976**, *102*, 1861–1877. [CrossRef]
17. Carlos Agustín, E. Estimation of Extreme Wind Speeds by Using Mixed Distributions. *Ing. Investig. Tecnol.* **2013**, *14*, 153–162. [CrossRef]
18. Tosunoğlu, F. Accurate estimation of T year extreme wind speeds by considering different model selection criterions and different parameter estimation methods. *Energy* **2018**, *162*, 813–824. [CrossRef]
19. Ulazia, A.; Sáenz, J.; Ibarra-Berastegi, G.; González-Rojí, S.J.; Carreno-Madinabeitia, S. Global estimations of wind energy potential considering seasonal air density changes. *Energy* **2019**, *187*, 115938. [CrossRef]
20. Wang, L.; Wang, Z.; Huang, N.; Fan, X.; Zhang, Z. Comparative analysis of cross-wind load code for high structures with circular sections. *Structures* **2022**, *43*, 1177–1186. [CrossRef]
21. Chen, F.; Wang, X.; Zhao, Y.; Li, Y.; Li, Q.; Xiang, P.; Li, Y.; Mazzotti, C. Study of Wind Loads and Wind Speed Amplifications on High-Rise Building with Opening by Numerical Simulation and Wind Tunnel Test. *Adv. Civ. Eng.* **2020**, *2020*, 8850688. [CrossRef]
22. Liang, Y.; Wu, C.; Ji, X.; Zhang, M.; Li, Y.; He, J.; Qin, Z. Estimation of the influences of spatiotemporal variations in air density on wind energy assessment in China based on deep neural network. *Energy* **2022**, *239*, 122210. [CrossRef]
23. Ren, G.; Wang, W.; Wan, J.; Hong, F.; Yang, K.; Yu, D. Investigating the impacts of spatial-temporal variation features of air density on assessing wind power generation and its fluctuation in China. *Sci. China Technol. Sci.* **2023**, *66*, 1797–1814. [CrossRef]
24. Liang, Y.; Ji, X.; Wu, C.; He, J.; Qin, Z. Estimation of the influences of air density on wind energy assessment: A case study from China. *Energy Convers. Manag.* **2020**, *224*, 113371. [CrossRef]
25. He, Y.C.; Lin, H.B.; Fu, J.Y.; Chan, P.W.; Zheng, Q.X.; Deng, T. Dependence of wind load on air density for highrise buildings. *J. Wind Eng. Ind. Aerodyn.* **2021**, *211*, 104558. [CrossRef]
26. Jung, C.; Schindler, D. The role of air density in wind energy assessment—A case study from Germany. *Energy* **2019**, *171*, 385–392. [CrossRef]
27. Bhatti, M.I.; Do, H.Q. Recent development in copula and its applications to the energy, forestry and environmental sciences. *Int. J. Hydrog. Energy* **2019**, *44*, 19453–19473. [CrossRef]
28. Wang, Y.; Ma, H.; Wang, D.; Wang, G.; Wu, J.; Bian, J.; Liu, J. A new method for wind speed forecasting based on copula theory. *Environ. Res.* **2018**, *160*, 365–371. [CrossRef]
29. Ding, Y.; Ye, X.; Guo, Y. Copula-based JPDF of wind speed, wind direction, wind angle, and temperature with SHM data. *Probabilistic Eng. Mech.* **2023**, *73*, 103483. [CrossRef]
30. Wang, H.; Xiao, T.; Gou, H.; Pu, Q.; Bao, Y. Joint distribution of wind speed and direction over complex terrains based on nonparametric copula models. *J. Wind Eng. Ind. Aerodyn.* **2023**, *241*, 105509. [CrossRef]
31. Bai, X.; Jiang, H.; Li, C.; Huang, L. Joint probability distribution of coastal winds and waves using a log-transformed kernel density estimation and mixed copula approach. *Ocean Eng.* **2020**, *216*, 107937. [CrossRef]
32. Wang, Z.; Zhang, W.; Tian, G.; Liu, Z. Joint values determination of wind and temperature actions on long-span bridges: Copula-based analysis using long-term meteorological data. *Eng. Struct.* **2020**, *219*, 110866. [CrossRef]
33. Chen, Y.; Chen, A.; Zhang, D. Evaluation of resources and environmental carrying capacity and its spatial-temporal dynamic evolution: A case study in Shandong Province, China. *Sustain. Cities Soc.* **2022**, *82*, 103916. [CrossRef]
34. Deng, X.; Gibson, J. Improving eco-efficiency for the sustainable agricultural production: A case study in Shandong, China. *Technol. Forecast. Soc.* **2019**, *144*, 394–400. [CrossRef]
35. Li, H.; Liu, S.; Yin, M.; Zhu, L.; Shen, E.; Sun, B.; Wang, S. Spatial and temporal variability and risk assessment of regional climate change in northern China: A case study in Shandong Province. *Nat. Hazards* **2022**, *111*, 2749–2786. [CrossRef]
36. Liang, Y.; Wu, C.; Zhang, M.; Ji, X.; Shen, Y.; He, J.; Zhang, Z. Statistical modelling of the joint probability density function of air density and wind speed for wind resource assessment: A case study from China. *Energy Convers. Manag.* **2022**, *268*, 116054. [CrossRef]

37. Gu, M.; Su, L.; Quan, Y.; Huang, J.; Fu, G. Experimental study on wind-induced vibration and aerodynamic mitigation measures of a building over 800 m. *J. Build Eng.* **2022**, *46*, 103681. [CrossRef]
38. Tian, Y.; Guan, H.; Shao, S.; Yang, Q. Provisions and comparison of Chinese wind load standard for roof components and cladding. *Structures* **2021**, *33*, 2587–2598. [CrossRef]
39. Jung, C.; Schindler, D. On the influence of wind speed model resolution on the global technical wind energy potential. *Renew. Sustain. Energy Rev.* **2022**, *156*, 112001. [CrossRef]
40. Zhang, Z.; Liang, Y.; Xue, X.; Li, Y.; Zhang, M.; Li, Y.; Ji, X. China's future wind energy considering air density during climate change. *Renew. Sustain. Energy Rev.* **2024**, *199*, 114452. [CrossRef]
41. Zhang, X.; Natarajan, A. Gaussian mixture model for extreme wind turbulence estimation. *Wind. Energy Sci.* **2022**, *7*, 2135–2148. [CrossRef]
42. Ye, X.W.; Xi, P.S.; Nagode, M. Extension of REBMIX algorithm to von Mises parametric family for modeling joint distribution of wind speed and direction. *Eng. Struct.* **2019**, *183*, 1134–1145. [CrossRef]
43. Jung, C.; Schindler, D. Wind speed distribution selection—A review of recent development and progress. *Renew. Sustain. Energy Rev.* **2019**, *114*, 109290. [CrossRef]
44. Da, L.; Yang, Q.; Liu, M.; Zhao, L.; Wu, T.; Chen, B. Estimation of extreme wind speed based on upcrossing rate of mean wind speeds with Weibull distribution. *J. Wind Eng. Ind. Aerodyn.* **2023**, *240*, 105495. [CrossRef]
45. Wang, Y.; Li, Y.; Zou, R.; Song, D. Bayesian infinite mixture models for wind speed distribution estimation. *Energy Convers. Manag.* **2021**, *236*, 113946. [CrossRef]
46. Lins, D.R.; Guedes, K.S.; Pitombeira-Neto, A.R.; Rocha, P.A.C.; de Andrade, C.F. Comparison of the performance of different wind speed distribution models applied to onshore and offshore wind speed data in the Northeast Brazil. *Energy* **2023**, *278*, 127787. [CrossRef]
47. Natarajan, N.; Vasudevan, M.; Rehman, S. Evaluation of suitability of wind speed probability distribution models: A case study from Tamil Nadu, India. *Environ. Sci. Pollut. Res. Int.* **2022**, *29*, 85855–85868. [CrossRef]
48. Poddaeva, O.; Fedosova, A. Extreme wind speeds analysis using extended wind rose based on statistic methods. *Energy Rep.* **2022**, *8*, 1177–81184. [CrossRef]
49. Gu, Y.; Fan, C.; Liang, L.; Zhang, J. Reliability calculation method based on the Copula function for mechanical systems with dependent failure. *Ann. Oper. Res.* **2022**, *311*, 99–116. [CrossRef]
50. Huang, Y.; Zhang, B.; Pang, H.; Wang, B.; Lee, K.Y.; Xie, J.; Jin, Y. Spatio-temporal wind speed prediction based on Clayton Copula function with deep learning fusion. *Renew. Energy* **2022**, *192*, 526–536. [CrossRef]
51. Ding, Y.; Ye, X.; Guo, Y. Wind load assessment with the JPDF of wind speed and direction based on SHM data. *Structures* **2023**, *47*, 2074–2080. [CrossRef]